Observation of an Internal *p-n* Junction in Pyrite FeS_2 Single Crystals: Origin of the Low Open Circuit Voltage in Pyrite Solar Cells

Bryan Voigt[1], William Moore[1], Moumita Maiti[1], Jeff Walter[1,2], Bhaskar Das[1], Michael Manno[1], Chris Leighton*[1], and Eray S. Aydil*[1,3]

[1]Department of Chemical Engineering and Materials Science,
University of Minnesota, Minneapolis, MN 55455, USA

[2]Department of Physics,
Augsburg University, Minneapolis, MN 55454, USA

[3]Department of Chemical and Biomolecular Engineering,
New York University Tandon School of Engineering, Brooklyn, NY 11201, USA

ABSTRACT: Pyrite FeS_2 has long been considered a potentially ideal photovoltaic material, but solar cells utilizing pyrite exhibit low open-circuit voltages (V_{OC}) and have failed to achieve conversion efficiencies >3 %. The recent discovery of a conductive *p*-type surface layer on *n*-type pyrite single crystals raises the intriguing possibility that the low V_{OC} results from a leaky internal *p-n* junction between the surface and interior. Here, we reveal this internal junction, for the first time, through horizontal electronic transport measurements on sulfur vacancy (V_S)- and Co-doped *n*-type pyrite single crystals. We observe a steep increase in resistance upon cooling heavily V_S-doped crystals below ~200 K, as the dominant charge transport crosses over from interior to surface conduction. The frequently employed two-resistor equivalent circuit model for lightly-doped pyrite crystals fails to reproduce this steep rise, but it can be accounted for, with high fidelity, by adding an internal Schottky junction resistance between the surface and the interior. The average extracted Schottky barrier height is 320 meV (varying from 130-560 meV), significantly below expectations from band bending calculations (>750 meV), but similar in magnitude to V_{OC} values reported for pyrite heterojunction solar cells. This internal *p-n* junction is thus directly implicated as the origin of the long-standing low-V_{OC} problem in pyrite.

Pyrite FeS_2 is a potentially ideal photovoltaic material for large-scale solar-to-electric power conversion because it is composed of non-toxic, sustainable, and inexpensive elements, has a suitable band gap (0.95 eV), and absorbs sunlight extremely strongly.[1,2] The inability to controllably dope pyrite, however, has precluded realization of pyrite *p-n* homojunction solar cells, and attempts at heterojunctions with various materials have consistently yielded disappointingly low efficiencies (≤ 3 %), limited by low open-circuit voltages (V_{OC}) < 0.3 V.[2–7] Numerous studies, going back 30 years, have thus focused on understanding the origin of this low V_{OC}.[2,4,6–9] While many hypotheses have emerged, a definitive explanation remains elusive, despite substantial ongoing interest in pyrite.[7,9–15]

Recent progress in understanding electronic transport in high quality pyrite single crystals, however, has provided perhaps the strongest clues to date.[9,16] Specifically, transport measurements on high-purity unintentionally-doped *n*-type pyrite single crystals have recently established a 1-3-nm-thick conductive surface layer. In as-grown crystals, this layer exhibits remarkable diversity in resistivity, varying by eight orders of magnitude at low temperatures (*e.g.*, $T < 30$ K), with both *n*- and *p*-type conduction, although *p*-type is most prevalent.[16] This diversity is suppressed when crystals are polished, yielding surface layers that appear to always be *p*-type,[2,9,16] likely due to surface states that pin the Fermi energy near the valence band.[2,9,16–18] Importantly, electronic transport in pyrite single crystals can be quantitatively described across a wide T range (1.8-700 K) using a model that includes two resistors in parallel, representing surface and interior contributions, respectively.[9,16] Notwithstanding this success, there remains an obvious inconsistency and a glaring open question in this context: with a *p*-type surface and an *n*-type interior, why have there been no indications in electronic transport of the internal *p-n* junction implied by their existence? More importantly, what would such a junction imply for the long-standing low V_{OC} problem?

Band bending calculations support the formation of the anticipated *p-n* junction (see Supporting Information Section A for calculation details). Figures 1a and 1b show, respectively, typical carrier densities and band bending near the surface of pyrite single crystals, as predicted by these calculations, and the equivalent circuit implied by their spatial variation. With typical parameters, a 12-nm-thick depletion region (light blue in Figure 1b) forms between the 5-nm-thick *p*-type surface layer (red in Figure 1b) and the *n*-type interior (dark blue in Figure 1b). This depletion region has not been detected in electronic transport measurements to date, however, nor included in transport models, as the latter typically only consider two resistors representing the crystal surface and interior.[9,16] The equivalent circuit for pyrite crystals (at small applied biases) should, instead, be as in Figure 1b, with resistors representing the *p-n* junctions. Since charge flowing through the crystal interior must necessarily pass through these internal junctions, the depletion region must surely contribute to the measured resistance. As already alluded to, a detailed understanding of transport across this region is important because a leaky internal junction, characterized by a low built-in potential, could be the origin of the problematic low V_{OC} in pyrite-based heterojunctions.[7,9]

Here, we present the first observation and detailed electrical characterization of this internal junction. Significantly, we show that the built-in potential (≤560 meV, on average ~320 meV) is substantially less than expected (>750 meV), and is typically on the order of the V_{OC} values observed in pyrite-based heterojunction solar and photoelectrochemical cells. The internal *p-n* junction is thus directly implicated as the origin of the long-standing low-V_{OC} problem in pyrite.

The observation of this internal *p-n* junction is made possible by our recent progress with understanding and controlling doping in pyrite single crystals.[19–21] Specifically, we have amassed substantial evidence that sulfur vacancies, V_S, (or their complexes)[21] are unintentional *n*-type dopants in pyrite.[19] We in fact

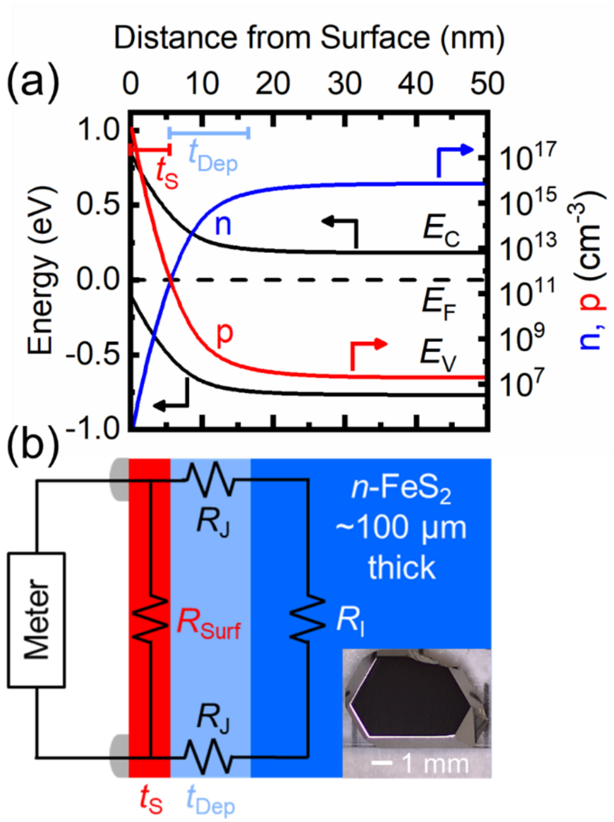

Figure 1. (a) Calculated band bending (left axis), and hole (*p*) and electron densities (*n*) (right axis), near the surface of a pyrite single crystal at 300 K. See Supporting Information Section A for calculation details. The surface layer ($t_S \approx 5.5$ nm) is defined as the region where $p>n$. The depletion layer thickness ($t_{Dep} \approx 12$ nm) is defined from the $p=n$ crossover point to the depth where $n = n_{Int}/e$, where n_{Int} is n deep in the interior. E_C, E_V, and E_F are the conduction band edge, valence band edge, and Fermi level, respectively. (b) Equivalent resistor network for a pyrite single crystal (bottom right) with resistors representing the *n*-type interior (R_I, dark blue), degenerately-doped *p*-type surface (R_{Surf}, red), and depletion region on the *n*-type side of the junction (R_J, light blue). The depletion region on the *p*-type side of the junction is thin (≤2 nm due to the heavy effective doping) and is thus ignored throughout this letter.

recently achieved control over the V_S density by growing pyrite single crystals in variable S vapor pressure, regulated *via* the molar ratio of S to Fe loaded into growth ampoules, hereafter referred to as the "S:Fe loading". Changing the S:Fe loading yields effective control over electronic properties, including resistivity (ρ), Hall electron density (*n*), and electronic thermal activation energy (ΔE). Lower S:Fe loadings, and thus lower S pressures, increase n(300 K) and decrease both ρ(300 K) and ΔE, consistent with V_S (or their complexes)[21] being *n*-type dopants. Critically, these trends are independent of metal impurity concentrations.[19] We build on these advances here to reveal the internal *p-n* junction in pyrite crystals by changing the V_S density, thus varying the interior resistivity over a wide range.

Pyrite single crystals were grown *via* chemical vapor transport (CVT). Growth details and extensive characterization of CVT crystals have been published.[16,19,20,22] In brief, polycrystalline phase-pure pyrite precursor powder was synthesized by heating a 6:1 molar ratio of S:Fe (99.9995% S, Alfa Aesar; 99.998 % Fe, Alfa Aesar) in evacuated and flame-sealed quartz ampoules to 500 °C for 6 days. With this pyrite powder as the source material and $FeBr_2$ as the transport agent, single crystals were grown, and V_S-doped during growth by varying the S vapor pressure *via* the total molar ratio of S:Fe loaded in the growth ampoules. S:Fe loadings of ≤2.0 were achieved by decomposing pyrite precursor in N_2 at temperatures of 350-600 °C into a mixture of pyrite and pyrrhotite (Fe_7S_8), and increased above 2.0 by adding excess S.[19] The S pressure during growth is estimated at 0.003 and 3.5 atm at low (≤2.0) and high (~3.0) S:Fe loading, respectively. Some crystals were also doped *n*-type with Co during growth (using conditions for light background V_S doping) by synthesizing pyrite precursor powder (99.99 % Fe, Sigma-Aldrich) with small amounts of Co to form ~5 at. % CoS_2; this was then ground thoroughly and used to spike growth ampoules.

Crystals were prepared for electronic transport measurements by visually identifying a {100} or {111} facet and polishing both sides using progressive grinding from 600 to 1500 grit SiC paper, followed by polishing with 3 μm- and 1 μm-diamond slurries. Contacts for transport measurements (van der Pauw resistivity and Hall effect)[23] were made in numerous ways including drying a Ag suspension (Ted Pella, product code: 16035), soldering (In), sputtering (Mg/Pt, Ni, Fe, Au), and evaporation (Co, Al). Soldered In was typically used, unless otherwise stated, though similar results were obtained for all contact materials and methods. Resistance measurements were made using DC with a Keithley 2400 or a combination of a Keithley 220 current source and 2002 voltmeter, or using AC with a Linear Research LR-700 resistance bridge (at 16 Hz). AC was specifically employed for resistances below ~1 Ω. Extensive checks for Ohmicity, Joule heating, and contact resistance were made. Most measurements were performed in a Quantum Design Physical Property Measurement System with a 9 T superconducting magnet, although occasional measurements were made in a closed-cycle He refrigerator with a 1 T electromagnet.

Evidence for the Internal Junction in Pyrite FeS_2

Figure 2 shows the *T*-dependence of the sheet resistance (R_S) for representative pyrite crystals grown at varied S:Fe loading. Figure S1 (Supporting Information Section B) shows the same data but as ρ(*T*), with ρ calculated from $\rho = R_S t$, where *t* is the crystal thickness (typically 100-1000 μm). For the crystal

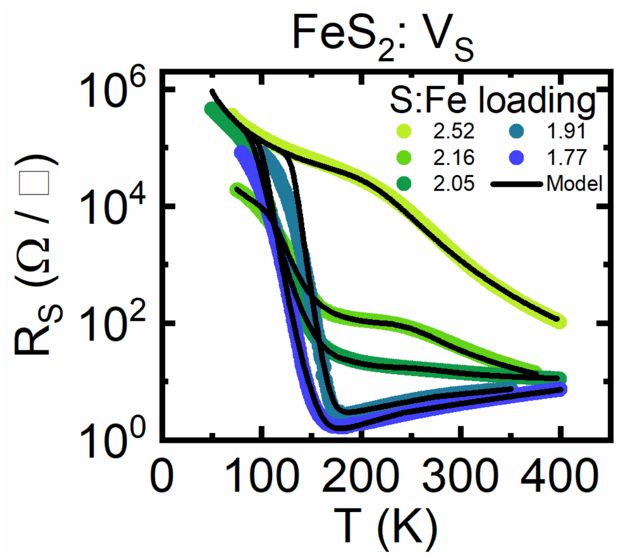

Figure 2. Temperature (T) dependence of the sheet resistance (R_S) for V_S-doped pyrite crystals. The V_S density is systematically increased by decreasing the S:Fe loading from 2.52 (light green data, low V_S doping) to 1.77 (blue data, high V_S doping). Equivalent resistor network (Figure 1b) model fits are shown as solid black lines for each crystal. Adapted with permission from (Voigt, B.; Moore, W.; Manno, M.; Walter, J.; Jeremiason, J.D.; Aydil, E.S.; Leighton, C. Transport Evidence for Sulfur Vacancies as the Origin of Unintentional *n*-Type Doping in Pyrite FeS_2. *ACS Appl. Mater. Interfaces* **2019**, 11, 15552-15563).[19] Copyright (2019) American Chemical Society.

grown at the highest S:Fe loading (2.52, lightest green line), R_S is ~1 kΩ/□ at 300 K and strongly T-dependent. Upon cooling, R_S increases until ~225 K, where the rate of increase slows as a function of T before accelerating again below ~175 K. This T-dependence is well understood to reflect a crossover from bulk conduction at high T to surface conduction at low T,[9,16] as charge carrier freeze-out in the interior allows surface conduction to shunt current flow and dominate R_S at low T. Freeze-out is strong in this lightly-V_S-doped crystal as V_S are deep donors, located ~0.23 eV below the conduction band minimum.[19] Increased V_S doping in Figure 2, achieved by progressively lowering the S:Fe loading (light green → dark blue curves), decreases R_S(300 K) by nearly three orders of magnitude and evolves the higher temperature transport from semiconducting (*i.e.*, negative dR_S/dT) to metallic-like (*i.e.*, positive dR_S/dT). This evolution in transport with S:Fe loading has been discussed previously in terms of approach to the insulator-metal transition.[19]

The feature in Figure 2 most relevant for this letter, and for the internal *p-n* junction, is the extraordinarily abrupt rise in R_S below ~200 K in crystals grown at S:Fe loadings <2.2. This steep rise is most prominent (spanning more than four orders of magnitude in ~60 K) in crystals with metallic-like high T transport (S:Fe loadings <2.0), where the interior becomes progressively more conductive upon cooling. The sharp increase eventually subsides on further cooling, when the transport crosses over to surface conduction at low T; as shown in Figure S2 (Supporting Information Section C), the nature of this low T surface conduction is essentially independent of V_S doping. This dramatic and unexpected rise in $R_S(T)$ is an important new observation because it cannot be described by the simple two-channel resistor model discussed above. If the two-parallel-resistor model typically used to describe pyrite[9,16] were sufficient, the crystal interior would continue to dominate transport at low T as it became even more conductive than at room temperature. This is clearly not the case, however. The precipitous rise in $R_S(T)$ instead indicates that current flow into the crystal is blocked by some additional resistance between the surface and the interior, not included in the two-parallel-resistor model. We thus interpret this strong increase in R_S below 200 K in heavily-V_S-doped crystals as the characteristic signature of an *internal p-n junction*, whose strongly T-dependent resistance cuts off transport through the conductive interior upon cooling, allowing surface conduction to dominate at low T (Figure 1). Importantly, this characteristic behavior in $R_S(T)$ is not affected by the contact material (Ag, Al, Au, Co, Fe, In, Ni, Mg/Pt) or how the contact was made (sputtering, evaporation, *etc.*). Figure S3 (Supporting Information Section D) shows $R_S(T)$ for heavily-V_S-doped crystals contacted by multiple materials, in multiple ways. Transport through the crystal interior is *always* lost upon cooling from 300 K, as the internal *p-n* junction cuts off the current, causing R_S to rise steeply before crossing over to surface conduction at low T. The insensitivity to contact material/method indicates that our findings are not compromised by some contact metal/pyrite (*i.e.*, external) junction effect. We contend that the presence of the "missing" internal junction in single crystal pyrite is the only simple interpretation of these data.

It is important to note that the indications of the internal junction in electronic transport are apparent only when pyrite crystals are heavily-V_S-doped and charge carrier freeze-out is eliminated, thus revealing the junction contribution to $R_S(T)$. Previous electronic transport measurements[7,9,16,24,25] were insensitive to this junction because of carrier freeze-out in the crystal interior, rendering the interior (as opposed to the junction) the largest contribution to $R_S(T)$ until sufficiently low T, where the surface shunts the current.

Junction Properties

We now demonstrate that quantitative modeling of $R_S(T)$ using the resistor network in Figure 1b allows for extraction of internal junction properties. This network comprises resistors representing the surface layer (R_{Surf}), the junction (R_J), and the crystal interior (R_I), each dominating R_S in heavily-V_S-doped crystals at low (<100 K), intermediate (100-200 K) and high (<300 K) temperatures, respectively. To extract junction properties from $R_J(T)$ in the intermediate T-range we exploit the fact that $R_S \approx R_{Surf}$ and $R_S \approx R_I$ in the low and high T limits, respectively, and that electronic transport in these limits is understood quantitatively.

The resistance of the *n*-type interior, R_I, can be described using a diffusive approach, *i.e.*, $R_I = (qn\mu t)^{-1}$, where q is the electronic charge, and $n(T)$ and $\mu(T)$ are the T-dependent electron density and mobility, respectively. The latter quantities, $n(T)$ and $\mu(T)$, can be obtained from Hall effect and resistivity measurements at high (>200 K) temperatures where the interior dominates transport. Figures 3a,e,i and 3b,f,j show $n(T)$ and $\mu(T)$, respectively, in representative crystals grown at high (a,b), moderate (e,f), and low (i,j) S:Fe loading, as well as fits to the data using $n(T) = n_\infty e^{-\Delta E/k_B T}$ and $\mu(T) = CT^{-\alpha}$. Here, k_B is Boltzmann's constant, C is a scaling factor, and n_∞, ΔE, and α are fitting parameters whose specific values are listed in Table

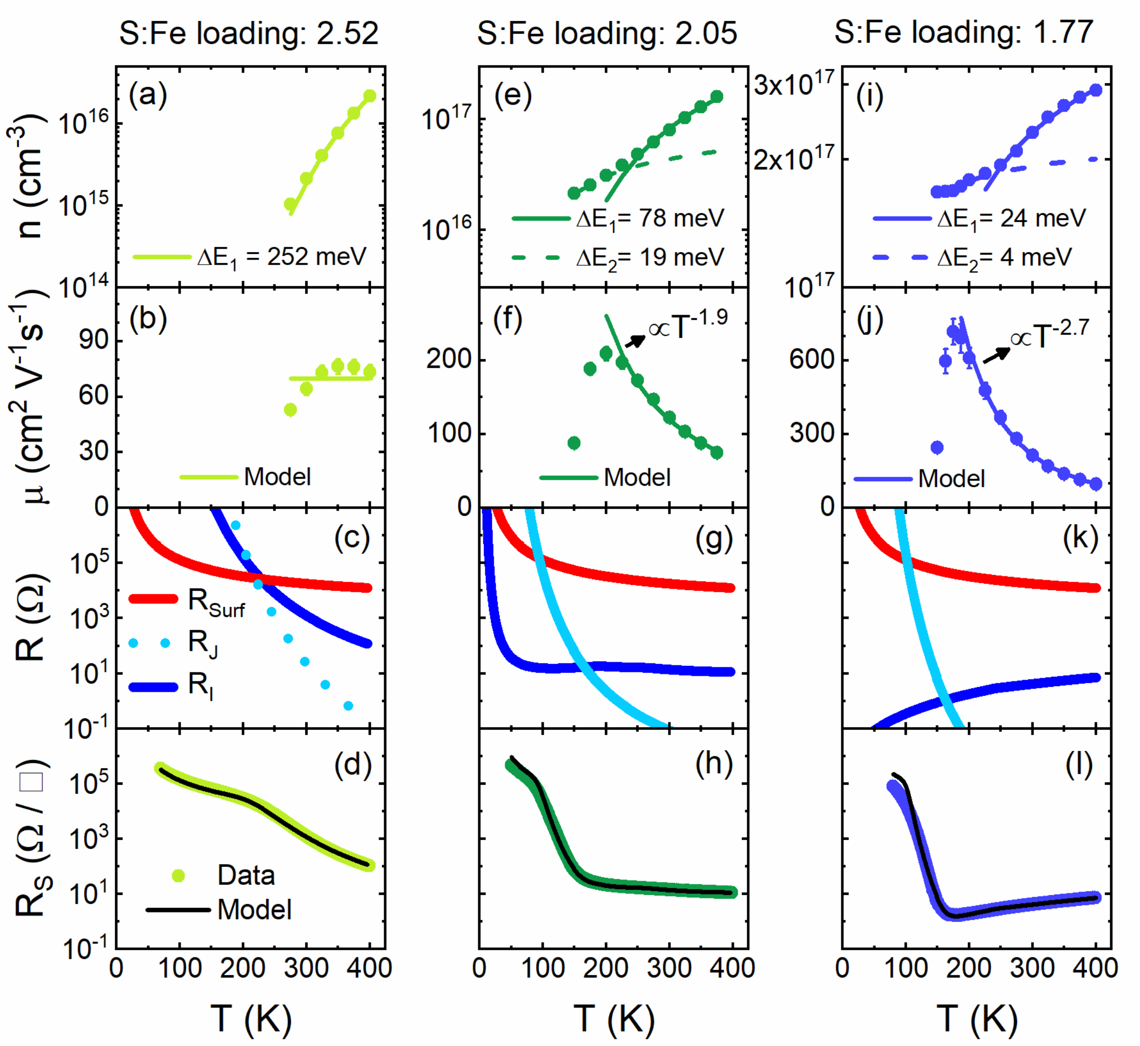

Figure 3. The temperature (T) dependence of transport properties (n and μ) and equivalent network resistor values (R_{Surf}, R_J, R_I, and R_S) that best fit the data for lightly- (S:Fe loading of 2.52, panels a-d), moderately- (S:Fe loading of 2.05, panels e-h), and heavily-V_S-doped crystals (S:Fe loading of 1.77, panels i-l). Experimental data are indicated with symbols; fits and modeled data are shown as lines. The shown activation energies (ΔE_i) are extracted from $n(T)$.

1 for the crystals in Figure 2. The rationale behind these functional forms, and other fitting details, are discussed in Supporting Information Section E. Briefly, the form of $n(T)$ (Figures 3a,e,i) accommodates two apparent activation energies (ΔE_1 and ΔE_2), each describing $n(T)$ in a different T range, as evident in Arrhenius plots of the same data (Supporting Information Section E, Figure S4). μ(T), on the other hand (Figures 3b,f,j), is limited by phonon scattering at high T and increases upon cooling, behavior that is typically modeled with a power law ($\mu(T) = CT^{-\alpha}$) where C is a constant and α is sensitive to the dominant phonon type.[9,16,26] Fitting parameters are again reported in Table 1 where α takes similar values to prior work.[9,16,27]

In contrast, the surface conduction at low T can be described by Efros-Shklovskii variable-range hopping (ES VRH), *i.e.*, $R_{\text{Surf}} = R_0 e^{(T_0/T)^{1/2}}$ where R_0 is the $T \to \infty$ extrapolation and T_0 is a characteristic temperature.[28] Previous work established this ES VRH as the dominant low T transport mechanism on-polished[9] and as-grown[16] pyrite crystal surfaces. We thus describe R_{Surf} using ES VRH with R_0 = 1200 Ω and T_0 = 2200 K (see Supporting Information Section F), unless specified otherwise. The resulting R_{Surf} is plotted in red in Figures 3c,g,k. For more details, and a discussion of how these quantities are obtained, see Supporting Information Sections C and F.

We next treat the interface region between the p-type surface layer and the n-type interior as a Schottky junction with barrier height φ_B, modeling the temperature-dependent junction resistance as $R_J(T) = R_{0,J} e^{q\varphi_B/k_B T}$, where $R_{0,J}$ is the $T \to \infty$ extrapolation of R_J.[26] (See Supporting Information Section G for more detailed discussion). In combination with $R_{\text{Surf}}(T)$ (described by ES VRH) and $R_I(T)$ (described by diffusive transport), $R_S(T)$ can now be modeled using the resistor network in Figure 1b, *with only two adjustable parameters* ($R_{0,J}$ and φ_B). The resulting junction resistances, $R_J(T)$, of crystals grown at high, moderate, and low S:Fe loading are shown as light blue lines (solid or dotted) in Figures 3c,g,k, respectively, along with $R_I(T)$ and $R_{\text{Surf}}(T)$. Generally, $R_I(T)$ evolves from insulating-like

Table 1. Summary of parameters in the equivalent resistor network model (Figure 1b) for the pyrite crystals in Figure 2.[a]

S:Fe loading	$R_{0,J}$ (Ω)	φ_B (meV)	ΔE_1 (meV)	$n_{\infty,1}$ (cm^{-3})	ΔE_2 (meV)	$n_{\infty,2}$ (cm^{-3})	α
1.77	5×10^{-9}	270	24	5.9×10^{17}	4 (242 K)	2.3×10^{17}	2.7
1.91	5×10^{-15}	500	45	4.1×10^{17}	23 (275 K)	1.7×10^{17}	2.9
2.05	1×10^{-4}	170	78	1.7×10^{18}	19 (235 K)	9×10^{16}	1.9
2.16	3×10^{-4}	170	155	1.0×10^{19}	23 (249 K)	2.1×10^{16}	1.4[b]
2.52	-	-	252	3.2×10^{19}	-	-	0

[a]$R_{0,J}$ is the extrapolated junction resistance in the infinite temperature ($T\rightarrow\infty$) limit, and φ_B is the barrier height. ΔE_i and $n_{\infty,i}$ are the activation energies and $T\rightarrow\infty$ electron densities, respectively, in the crystal interior, in the two distinct T regimes (i = 1 or 2 denotes the higher- and lower-T regimes, respectively), and the T listed beneath ΔE_2 is where the two regimes intersect and crossover. α is the exponent in $\mu \propto T^{-\alpha}$.

[b]Here only, the mobility is modeled (using Matthiesen's rule) as $\mu(T)^{-1} = (CT^{-\alpha})^{-1} + (DT^{\beta})^{-1}$, where the latter term, including D, a prefactor, and β, an exponent, represents ionized impurity scattering; β = 2.1 is used. See Supporting Information Section E for more details.

to metallic-like with decreasing S:Fe loading (higher V_S doping), while $R_{Surf}(T)$ remains constant. The difference between $R_I(T)$ and $R_{Surf}(T)$ thus becomes increasingly apparent in Figures 3c,g,k, leading to progressively more dramatic rises in $R_S(T)$ (Figure 3d,h,l) when $R_J(T)$ dominates at intermediate T. Note that at the highest S:Fe loading (Figure 3c), $R_J(T)$ is shown as a dotted light blue line to indicate that inclusion of this resistance is no longer necessary for quantitative description of $R_S(T)$, because conduction in the crystal interior switches smoothly to surface conduction as the carriers freeze-out upon cooling, with no clear indication of the junction. In essence, at high T, the junction resistance in this case is too low to influence current flow into the crystal interior, while at low T carrier freeze-out has already prevented current flow through the bulk; high junction resistance is thus irrelevant in this regime. An upper bound on φ_B of 500 meV can be established at this V_S doping by increasing φ_B until $R_J(T)$ begins to affect the model-prediction for $R_S(T)$ (Supporting Information Section G).

With these three contributions in hand, the $R_S(T)$ of lightly, moderately, and heavily doped crystals can be calculated and are shown as black lines in Figures 3d,h,l, respectively. The new model that includes the junction resistance is found to describe $R_S(T)$ with high fidelity across a wide range of V_S doping, providing strong quantitative evidence for the validity of the equivalent circuit model in Figure 1b, and the first direct quantitative transport evidence for the presence of an internal *p-n* junction in pyrite. The $R_{0,J}$ and φ_B extracted from the experimental measurements are shown in Table 1. As shown in Figure 4, which expands such data to 19 studied crystals, the majority of the extracted φ_B values range from 170-400 meV (average ~320 meV), significantly less than anticipated from band bending. For example, in heavily-V_S-doped crystals (*e.g.*, S:Fe loadings <2.0), φ_B should be ≥750 meV based on band bending (Supporting Information Section A). Of the 19 crystals measured and analyzed in this work, φ_B exceeds 400 meV in five samples (*e.g.*, the φ_B = 500 meV shown in Table 1), the largest being 560 meV. Notably, a distribution (Figure 4) of φ_B values is obtained, even when the crystals have nominally identical interior V_S doping and surface preparation. While there is no readily apparent detailed explanation for these differences, these junction barrier heights would be expected to be sensitive to variations in parameters such as defect densities (and their spatial dependence) in the internal junction region. Regardless, the φ_B values extracted indicate a loss in internal junction potential of at least 200 meV, in most cases substantially more. These smaller-than-expected φ_B are direct evidence of a significant deficit in barrier height. Moreover, the striking similarity between the magnitudes of φ_B and the V_{OC} values observed in pyrite heterojunction single crystal solar cells[2–7] (Figure 4) implicates this internal junction as the likely culprit for the low V_{OC} in pyrite solar cells. In simple terms, prior single crystal pyrite Schottky solar cells, for example,[6] likely generated effectively metal-metal contacts between the overlying metal and the heavily *p*-doped pyrite surface, the observed (low) V_{OC} arising at the (leaky) internal *p-n* junction. Clearly, studies investigating which factors influence φ_B could advance our understanding and provide strategies for mitigating the observed voltage deficit. The work outlined here unveiling this internal junction lays the foundation for such an effort.

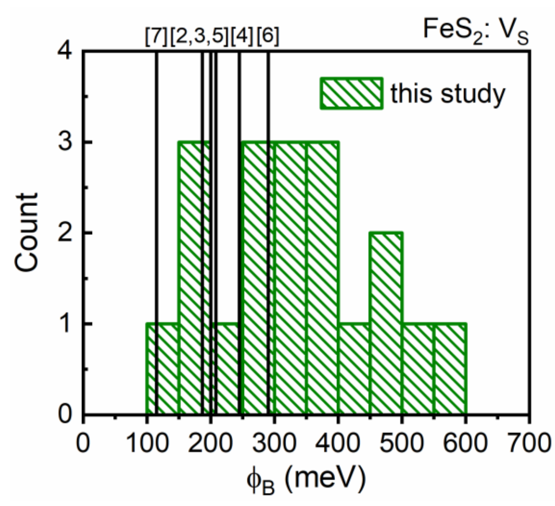

Figure 4. Histogram of Schottky barrier heights (φ_B) extracted from $R_S(T)$ of 19 different V_S-doped crystals. For comparison, vertical lines denote the largest V_{OC} obtained in past reports on pyrite single crystal heterojunction solar cells (reference numbers labeled).

Barrier Control: Co-doped FeS_2

Yet heavier doping than achieved with the lowest S:Fe loading here (*i.e*., the highest V_S doping) would be expected to eliminate the internal junction by steepening the band bending, narrowing the depletion region, suppressing the thermionic emission component of the junction, promoting tunneling transport, and eventually creating an Ohmic contact to the interior of the crystal.[26] The highest electron density achieved to date with V_S doping of high purity pyrite crystals is $n(300\text{ K}) \approx 2\times10^{17}$ cm^{-3}, however, as V_S are deep donors.[19] An alternative approach to increasing electron densities beyond this is doping with Co, a known shallow donor in pyrite.[29–32] We thus tested this expectation by Co-doping during crystal growth, under conditions that otherwise result in light V_S doping ($n(300\text{ K}) < 10^{16}$ cm^{-3}). As shown in Figure 5, Co-doping increases $n(300\text{ K})$ by three orders of magnitude and decreases $R_S(300\text{ K})$ by four orders of magnitude, confirming that Co is an effective *n*-dopant. As the Co-doping is increased, $R_S(T)$ evolves from exhibiting bulk freeze-out in crystals with no intentional Co-doping (red curve) to nearly-*T*-independent R_S in moderately-Co-doped crystals ($R_S(300\text{ K}) = 1\text{-}100\ \Omega$). The latter crystals clearly display the influence of the junction upon cooling below ~200 K, before giving way to surface conduction at low *T*, consistent with our heaviest V_S-doped crystals. Importantly, however, with further Co-doping (black curve), to $n(300\text{ K}) > 10^{18}$ cm^{-3}, the signature of the internal junction, *i.e.*, the steep rise below 200 K, disappears in $R_S(T)$ and transport through the interior is accessed at all *T*. This confirms expectations and provides further evidence that a mitigable internal *p-n* junction exists in pyrite single crystals. In these highest doped crystals, finite R_S at low *T* in fact indicates metallic behavior; the surface-interior junction is thus now a metal-metal junction, forming an Ohmic contact. At such heavy Co-doping, calculations show that >90 % of the band bending occurs within ~12 nm of the crystal surface (Supporting Information Section H, Figure S5a). For comparison, in

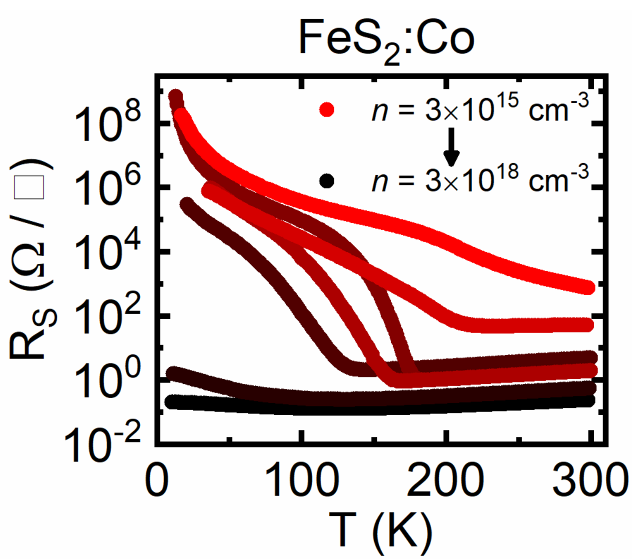

Figure 5. The temperature (*T*) dependence of sheet resistance (R_S) for Co-doped pyrite single crystals. $R_S(T)$ is shown for crystals grown with increasing Co doping using a color gradient from red ($n(300\text{ K}) = 3\times10^{15}$ cm^{-3} (due to background V_S)) to black (heavy Co doping to $n(300\text{ K}) = 3\times10^{18}$ cm^{-3}).

Au/Si Schottky diodes (with $\varphi_B \approx 0.8$ eV[33] and assuming a hydrogenic donor with density $N_D \approx 3\times10^{18}$ cm^{-3}), tunneling dominates transport across the junction when $N_D > 10^{18}$ cm^{-3},[26] and >90 % of band bending is within ~14 nm of the Si surface (Supporting Information Section H, Figure S5b). With similarly sharp band bending in pyrite crystals we thus expect tunneling to be facile, and to dominate the transport across the junction, allowing unimpeded charge flow from the surface to the interior at all temperatures. We note that the similar band bending (effectively, t_{Dep}) between Si and FeS_2 is a result of coincidentally similar quotients of each material's dielectric constant to donor density.

Finally, we note that we also considered and conducted vertical transport measurements to attempt to further characterize the observed junction. Several challenges were encountered, however. As an example, the current in such measurements must flow through two face-to-face junctions. Such measurements have been made in other systems,[34–36] but this nevertheless greatly complicates experiments and interpretation unless one (and only one) junction can be mitigated. Furthermore, the relatively small φ_B (~300 meV) precludes extraction of useful information from vertical transport measurements at 300 K. While cooling would increase the influence of this junction, forming Ohmic contacts then becomes a challenge. The horizontal transport measurements presented here, on the other hand, are ideal for probing the internal junction as van der Pauw sheet resistance measurements eliminate contact contributions.[23]

In summary, horizontal charge transport measurements in heavily V_S- and Co-doped pyrite single crystals evidence an internal *p-n* junction, specifically *via* a dramatic rise in resistance on cooling that cannot be modeled by a simple two-resistor model where the resistors represent surface and interior conduction. This steep rise *can* be accounted for, however, by adding a Schottky junction resistance between the surface and interior. This new equivalent circuit network describes the pyrite single crystal sheet resistance across the entire temperature range studied, from 10-400 K. Junction barrier heights extracted from such data amount to 320 meV on average, significantly less than the band bending expected at the pyrite surface (>750 meV) but remarkably similar to the typical low V_{OC} values reported for past pyrite single crystal solar cells. This lends strong credence to the hypothesis that an internal *p-n* junction, detected unequivocally for the first time here, is responsible for the historically low efficiencies in pyrite-based heterojunction solar cells.

ASSOCIATED CONTENT

SUPPORTING INFORMATION

The Supporting Information is available free of charge at http://pubs.acs.org.

Band bending calculation details, resistivity data, hopping conduction analysis, contact-dependence of sheet resistance, Arrhenius fits to the electron density, circuit network model details, band bending calculations of Co-doped pyrite and Au/Si Schottky contacts (PDF)

AUTHOR INFORMATION

Corresponding Authors

Eray S. Aydil – New York University, Brooklyn, NY, USA; Email: aydil@nyu.edu

Chris Leighton – University of Minnesota, Minneapolis, MN, USA; orcid.org/0000-0003-2492-0816; Email: leighton@umn.edu

Author Contributions

E.S.A. and C. L. conceived of the study and oversaw its execution. B.V., W.M., B.D., and M. Manno grew the crystals. B.V., W.M., M. Maiti, and B.D. performed electrical transport measurements, with guidance from J.W. and M. Manno. B.V., E.S.A., and C.L. wrote the paper, with input from all other authors. All authors have given approval to the final version of the manuscript.

Funding Sources

Work supported by the customers of Xcel Energy through a grant from the Renewables Development Fund, and in part by the National Science Foundation (NSF) through the University of Minnesota MRSEC under DMR-1420013. Work on Co-doped FeS_2 was supported by the US Department of Energy (DOE) through the University of Minnesota Center for Quantum Materials under DE-SC-0016371.

Notes

The authors declare no competing financial interest.

ACKNOWLEDGMENT

We thank D. Ray, L. Gagliardi, and J. Batley for informative discussions. We also thank J. Batley for evaporation of Co and Al contacts.

ABBREVIATIONS

V_{OC}, open-circuit voltage; V_S, sulfur vacancies; ρ, resistivity; T, temperature; E_F, Fermi level; E_C, conduction band edge energy; E_V, valence band edge energy; n, Hall electron density; p, Hall hole density; μ, Hall mobility; ΔE, electron thermal activation energy; CVT, chemical vapor transport; R_S, sheet resistance; R_{Surf}, surface resistance; R_J, junction resistance; R_I, interior (or bulk) resistance; ES VRH, Efros-Shklovskii variable-range hopping; φ_B, Schottky barrier height; $R_{0,J}$, temperature→∞ junction resistance; t, crystal thickness; t_S, surface layer thickness; t_{Dep}, depletion layer thickness

REFERENCES

(1) Wadia, C.; Alivisatos, A. P.; Kammen, D. M. Materials Availability Expands the Opportunity for Large-Scale Photovoltaics Deployment. *Environ. Sci. Technol.* **2009**, *43*, 2072–2077.

(2) Ennaoui, A.; Fiechter, S.; Pettenkofer, C.; Alonso-Vante, N.; Büker, K.; Bronold, M.; Höpfner, C.; Tributsch, H. Iron Disulfide for Solar Energy Conversion. *Sol. Energy Mater. Sol. Cells* **1993**, *29*, 289–370.

(3) Ennaoui, A.; Tributsch, H. Iron Sulphide Solar Cells. *Sol. Cells* **1984**, *13*, 197–200.

(4) Ennaoui, A.; Tributsch, H. Energetic Characterization of the Photoactive FeS_2 (Pyrite) Interface. *Sol. Energy Mater.* **1986**, *14*, 461–474.

(5) Ennaoui, A.; Fiechter, S.; Jaegermann, W.; Tributsch, H. Photoelectrochemistry of Highly Quantum Efficient Single-Crystalline n-FeS_2 (Pyrite). *J. Electrochem. Soc.* **1986**, *133*, 97–106.

(6) Büker, K.; Alonso-Vante, N.; Tributsch, H. Photovoltaic Output Limitation of n-FeS_2 (Pyrite) Schottky Barriers: A Temperature-Dependent Characterization. *J. Appl. Phys.* **1992**, *72*, 5721–5728.

(7) Cabán-Acevedo, M.; Kaiser, N. S.; English, C. R.; Liang, D.; Thompson, B. J.; Chen, H.; Czech, K. J.; Wright, J. C.; Hamers, R. J.; Jin, S. Ionization of High-Density Deep Donor Defect States Explains the Low Photovoltage of Iron Pyrite Single Crystals. *J. Am. Chem. Soc.* **2014**, *136*, 17163–17179.

(8) Bronold, M.; Pettenkofer, C.; Jaegermann, W. Surface Photovoltage Measurements on Pyrite (100) Cleavage Planes: Evidence for Electronic Bulk Defects. *J. Appl. Phys.* **1994**, *76*, 5800–5808.

(9) Limpinsel, M.; Farhi, N.; Berry, N.; Lindemuth, J.; Perkins, C. L.; Lin, Q.; Law, M. An Inversion Layer at the Surface of n-Type Iron Pyrite. *Energy Environ. Sci.* **2014**, *7*, 1974–1989.

(10) Shukla, S.; Xing, G.; Ge, H.; Prabhakar, R. R.; Mathew, S.; Su, Z.; Nalla, V.; Venkatesan, T.; Mathews, N.; Sritharan, T.; et al. Origin of Photocarrier Losses in Iron Pyrite (FeS_2) Nanocubes. *ACS Nano* **2016**, *10*, 4431–4440.

(11) Wu, L.; Dzade, N. Y.; Gao, L.; Scanlon, D. O.; Ozturk, Z.; Hollingsworth, N.; Weckhuysen, B. M.; Hensen, E. J. M.; de Leeuw, N. H.; Hofmann, J. P. Enhanced Photoresponse of FeS_2 Films: The Role of Marcasite-Pyrite Phase Junctions. *Adv. Mater.* **2016**, *28*, 9602–9607.

(12) Rhodes, J. M.; McBride, J. R.; Macdonald, J. E. Synthesis of FeS_2-CoS_2 Core-Frame and Core-Shell Hybrid Nanocubes. *Chem. Mater.* **2018**, *30*, 8121–8125.

(13) McAuliffe, R. D.; Shoemaker, D. P. Inflexible Stoichiometry in Bulk Pyrite FeS_2 as Viewed by *in Situ* and High-Resolution X-Ray Diffraction. *Acta Crystallogr. Sect. B Struct. Sci. Cryst. Eng. Mater.* **2018**, *74*, 436–444.

(14) Roberts, D. M.; Russek, S. E.; Stoldt, C. R. Synthetic Iron Pyrite Across Length Scales: Interfacial Defects and Macroscopic Properties. *CrystEngComm* **2019**, *21*, 3304–3312.

(15) Moon, D. G.; Rana, T. R.; Rehan, S.; Haider Naqvi, S. D.; Siddique, Y.; Lee, S. M.; Ahn, S. K.; Cho, Y. S.; Ahn, S. Na-Mediated Stoichiometry Control of FeS_2 Thin Films: Suppression of Nanoscale S-Deficiency and Improvement of Photoresponse. *ACS Appl. Mater. Interfaces* **2019**, *11*, 43244–43251.

(16) Walter, J.; Zhang, X.; Voigt, B.; Hool, R.; Manno, M.; Mork, F.; Aydil, E. S.; Leighton, C. Surface Conduction in n-Type Pyrite FeS_2 Single Crystals. *Phys. Rev. Mater.* **2017**, *1*, 065403.

(17) Bronold, M.; Buker, K.; Kubala, S.; Pettenkofer, C.; Tributsch, H. Surface Preparation of FeS_2 via Electrochemical Etching and Interface Formation with Metals. *Phys. Status Solidi* **1993**, *135*, 231–243.

(18) Bronold, M.; Tomm, Y.; Jaegermann, W. Surface States on Cubic d-Band Semiconductor Pyrite (FeS_2). *Surf. Sci.* **1994**, *314*, L931–L936.

(19) Voigt, B.; Moore, W.; Manno, M.; Walter, J.; Jeremiason, J. D.; Aydil, E. S.; Leighton, C. Transport Evidence for Sulfur Vacancies as the Origin of Unintentional n-Type Doping in Pyrite FeS_2. *ACS Appl. Mater. Interfaces* **2019**, *11*, 15552–15563.

(20) Zhang, X.; Li, M.; Walter, J.; O'Brien, L.; Manno, M. A.; Voigt, B.; Mork, F.; Baryshev, S. V.; Kakalios, J.; Aydil, E. S.; Leighton, C. Potential Resolution to the Doping Puzzle in Iron Pyrite: Carrier Type Determination by Hall Effect and Thermopower. *Phys. Rev. Mater.* **2017**, *1*, 015402.

(21) Ray, D.; Voigt, B.; Manno, M.; Aydil, E. S.; Leighton, C.; Gagliardi, L. unpublished.

(22) Zhang, X.; Scott, T.; Socha, T.; Nielsen, D.; Manno, M.; Johnson, M.; Yan, Y.; Losovyj, Y.; Dowben, P.; Aydil, E. S.; Leighton, C. Phase Stability and Stoichiometry in Thin Film Iron Pyrite: Impact on Electronic Transport Properties. *ACS Appl. Mater. Interfaces* **2015**, *7*, 14130–14139.

(23) van der Pauw, L. J. Method of Measuring Specific Resistivity and Hall Effect of Discs of Arbitrary Shape. *Philips Res. Reports* **1958**, *13*, 1–9.

(24) Willeke, G.; Blenk, O.; Kloc, C.; Bucher, E. Preparation and Electrical Transport Properties of Pyrite (FeS_2) Single Crystals. *J. Alloys Compd.* **1992**, *178*, 181–191.

(25) Schieck, R.; Hartmann, A.; Fiechter, S.; Könenkamp, R.; Wetzel, H. Electrical Properties of Natural and Synthetic Pyrite (FeS_2) Crystals. *J. Mater. Res.* **1990**, *5*, 1567–1572.

(26) Sze, S. M. *Physics of Semiconductor Devices*; Sons, J. W. &, Ed.; New York, 1981.

(27) Tomm, Y.; Schieck, R.; Ellmer, K.; Fiechter, S. Growth Mechanism and Electronic Properties of Doped Pyrite (FeS_2) Crystals. *J. Cryst. Growth* **1995**, *146*, 271–276.

(28) Shklovskii, B. I.; Efros, A. L. *Electronic Properties of Doped Semiconductors*; Springer: Berlin, 1984.

(29) Lehner, S. W.; Savage, K. S.; Ayers, J. C. Vapor Growth and Characterization of Pyrite (FeS_2) Doped with Co, Ni, and As: Variations in Semiconducting Properties. *J. Cryst. Growth* **2006**, *286*, 306–317.

(30) Guo, S.; Young, D. P.; Macaluso, R. T.; Browne, D. A.; Henderson, N. L.; Chan, J. Y.; Henry, L. L.; Ditusa, J. F. Discovery of the Griffiths Phase in the Itinerant Magnetic Semiconductor $Fe_{1-x}Co_xS_2$. *Phys. Rev. Lett.* **2008**, *100*, 017209.

(31) Guo, S.; Young, D. P.; Macaluso, R. T.; Browne, D. A.; Henderson, N. L.; Chan, J. Y.; Henry, L. L.; Ditusa, J. F. Charge Transport in Cobalt-Doped Iron Pyrite. *Phys. Rev. B* **2010**, *81*, 144424.

(32) Lehner, S. W.; Newman, N.; Van Schilfgaarde, M.; Bandyopadhyay, S.; Savage, K.; Buseck, P. R. Defect Energy Levels and Electronic Behavior of Ni-, Co-, and As-Doped Synthetic Pyrite (FeS_2). *J. Appl. Phys.* **2012**, *111*, 083717.

(33) Chang, C. Y.; Sze, S. M. Carrier Transport Across Metal-Semiconductor Barriers. *Solid. State. Electron.* **1970**, *13*, 727–740.

(34) Hernández-Ramírez, F.; Tarancón, A.; Casals, O.; Rodríguez, J.; Romano-Rodríguez, A.; Morante, J. R.; Barth, S.; Mathur, S.; Choi, T. Y.; Poulikakos, D.; Callegari, V.; Nellen, P. M. Fabrication and Electrical Characterization of Circuits Based on Individual Tin Oxide Nanowires. *Nanotechnology* **2006**, *17*, 5577–5583.

(35) Zhang, Z.; Yao, K.; Liu, Y.; Jin, C.; Liang, X.; Chen, Q.; Peng, L. M. Quantitative Analysis of Current-Voltage Characteristics of Semiconducting Nanowires: Decoupling of Contact Effects. *Adv. Funct. Mater.* **2007**, *17*, 2478–2489.

(36) Chiquito, A. J.; Amorim, C. A.; Berengue, O. M.; Araujo, L. S.; Bernardo, E. P.; Leite, E. R. Back-to-Back Schottky Diodes: The Generalization of the Diode Theory in Analysis and Extraction of Electrical Parameters of Nanodevices. *J. Phys. Condens. Matter* **2012**, *24*, 225303.

Graphic entry for the Table of Contents (TOC):